

Single-Site Emitter Localization via Multipath Fingerprinting

Evgeny Kupershtein, Mati Wax, *Fellow, IEEE*, and Israel Cohen, *Senior Member, IEEE*

Abstract—A novel method enabling single-site localization of wireless emitters in a rich multipath environment is presented. The localization is based on a novel fingerprinting technique exploiting the spatial-temporal characteristics of the multipath signals received by the base station antenna array. The fingerprint is based on a lower dimensional signal subspace of the spatial-temporal covariance matrix, capturing the dominant multipath signals. The performance is validated with both simulated and real data, demonstrating localization accuracy of about 1 m in typical indoor environments.

Index Terms—Antenna array, indoor localization, multipath fingerprinting, signal subspace.

I. INTRODUCTION

POSITION location of a wireless emitter is an old and well-investigated problem with both military and commercial applications. Many techniques have been developed to solve this problem over the last 60 years, most of them based on the assumption that the wireless signal travels from the source to the receiving antennas along the line-of-sight (LOS) path connecting them. The classical position location techniques, direction-of-arrival (DOA), time-of-arrival (TOA) and differential-time-of-arrival (DTOA), are all based on this assumption, with the localization carried out via triangulation, using several such measurements [1], [2].

In recent years there has been a growing interest in position location in urban canyons and in indoor venues, where LOS conditions usually do not exist. In these cases, the propagation from the source to the receiving antennas is usually made through reflections from buildings and walls, referred to as multipath, which may be very different from the LOS path. As a result, the

classical position location techniques are not valid in such scenarios.

Fingerprinting techniques have been recently developed [3]–[25] to overcome this problem. Fingerprinting techniques are based on the premise that there is a one-to-one relation between the characteristics of the signals received at the base stations and the emitter location, i.e., that a fingerprint can be extracted from the received signals and serve as a unique identifier of the emitter location. The problem is casted as a pattern recognition problem, namely, a database of fingerprints is pre-collected in the desired coverage area, and the location is determined by matching the extracted fingerprint to the fingerprint database.

Two types of fingerprinting techniques have been developed about the same time. The first, developed by Wax *et al.* [3]–[6] and further investigated by Nezafat *et al.* [7]–[9], is based on using the multipath characteristics, derived from the signals received by a multiple-antenna base station (BS), as the location fingerprint. A review of this technique, referred to as “Location Fingerprinting”, was first presented in [10]. The second technique, developed by Bahl and Padmanabhan [11] and by Laitinen *et al.* [12], is based on using the received signal strength (RSS) obtained at several base stations as the location fingerprint.

The RSS fingerprint depends on many irrelevant parameters such as the orientation of the transmitter and body shadowing, but more critically, suffers from high variability along a short distance of wavelength because of constructive and destructive multipath interferences. As a result, the accuracy of this technique is limited and requires signal strength measurements from multiple BSs to assure an acceptable accuracy. The multipath based fingerprint, on the other hand, exploits the multipath to its advantage, rather than suffers from it, thus enabling a much higher accuracy.

The work of Wax *et al.* in [3]–[5] was focused on the outdoor environment and confined to narrowband signals (AMPS) and used a fingerprint based on the directions-of-arrival of the multipath signals. In [6] Wax *et al.* extended their work to wide-band signals (CDMA) by adding another fingerprint based on the power delay profile (PDP) of the multipath signals. The idea of using the PDP as a fingerprint was also investigated by Nypan *et al.* [13], Ahonen and Laitinen [14] and Ahonen and Eskelinen [15]. Meurer *et al.* [16] proposed using the covariance matrix of the channel impulse response (CIR) as a location fingerprint rather than the power delay profile. Triki, Oktem and Slock [17]–[19] have extended the PDP fingerprinting in several aspects, including adding to the fingerprint the spatial information of the antenna array, in both receive and transmit (MIMO),

Manuscript received March 11, 2012; revised September 01, 2012; accepted September 03, 2012. Date of publication October 03, 2012; date of current version December 04, 2012. The associate editor coordinating the review of this manuscript and approving it for publication was Prof. Jean Pierre Delmas. This research was supported in part by Alvarion and the Israel Science Foundation (grant no. 1130/11).

E. Kupershtein is with the Electrical Engineering Department, Technion—Israel Institute of Technology, Haifa 32000, Israel, and also with Alvarion, Yoqneam-Illit 20692, Israel (e-mail: gskuper@gmail.com).

M. Wax is with Alvarion, Yoqneam-Illit 20692, Israel. (e-mail: mati.wax@alvarion.com).

I. Cohen is with the Electrical Engineering Department, Technion—Israel Institute of Technology, Technion City, Haifa 32000, Israel (e-mail: icohen@ee.technion.ac.il).

Color versions of one or more of the figures in this paper are available online at <http://ieeexplore.ieee.org>.

Digital Object Identifier 10.1109/TSP.2012.2222395

as well as the Doppler shifts of the different reflections, for the case that the mobile terminal is moving. The asymptotic performance of the PDP method was investigated under various statistical models by Oktem and Slock [20], [21]. The applicability of PDP fingerprinting for UWB localization was investigated by Altahus *et al.* [22], Steiner and Wittneben [23], [24].

The current work extends the work of Wax *et al.* [3]–[6] in several aspects. First, it presents a novel and more powerful fingerprint that exploits both the directions-of-arrival and the differential-delays of the multipath signals. This fingerprint is based on a lower dimensional subspace of the spatial-temporal covariance matrix wherein the multipath signals reside, commonly referred to as the signal subspace. The subspace estimation does not require estimation of the directions-of-arrival and differential-delays of the multipath reflections, which is both difficult and computationally intensive problem in rich multipath environments. Moreover, the subspace captures only the dominant reflections, thus forming both rich and robust fingerprint that enables, in conjunction with the powerful similarity-profile matching criterion, accurate single-site localization. Second, it presents necessary and sufficient conditions that guarantee unique localization. Third, unlike [6], this method is applicable to any wideband signal with a repeatable segment. As such, it is applicable to most modern communication techniques, since they all use a fixed and repeatable segment of the signal for synchronization and channel estimation purposes. As shown in the Appendix, this method is applicable also to localization using the array channel impulse response (CIR). In addition, unlike [3]–[6], this work is focused on the indoor environment, yet applicable also to outdoor environments. Even though both environments are characterized by rich multipath, the indoors multipath environment is typically richer and characterized by a larger angle spread and smaller delay spread.

A general view of the proposed localization method is presented in Fig. 1. The technique consists of two phases: an off-line phase and an on-line phase. During the off-line phase, a database of multipath fingerprints is collected in the desired coverage area, with the fingerprint extracted from the BS antenna array signals. In the on-line phase, the multipath fingerprint is extracted from the BS antenna array signals and matched to the fingerprints stored in the database. The location whose fingerprint best matches the extracted fingerprint is selected as the emitter location.

The outline of the rest of the paper is as follows. In Sections II and III we present the problem formulation and the conditions for unique localization. Then, in Sections IV and V we present the similarity-metric derivation and the signal subspace based localization method. Sections VI and VII present test results with simulated and real data. Finally, in Sections VIII and IX we present the discussion and the conclusions.

II. PROBLEM FORMULATION

Consider an array composed of p sensors with arbitrary locations and arbitrary directional characteristics receiving a wideband signal $s(t)$, centered at frequency $\omega_c = 2\pi f_c$, impinging

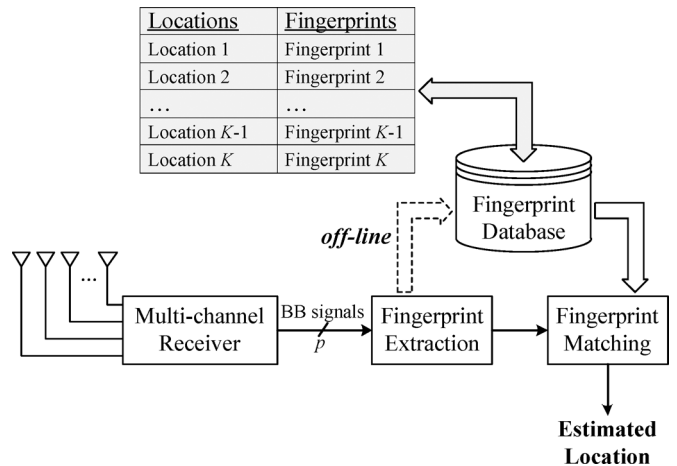


Fig. 1. Block diagram of the proposed localization technique.

on the array through q reflections with time delays τ_1, \dots, τ_q , and corresponding directions $\theta_1, \dots, \theta_q$. The outputs of the antenna array are sampled simultaneously at N times (“taps”), with an interval of $D = 1/BW$ seconds, i.e., each sensor is sampled at times $(t + \ell D)$, $\ell = 0, \dots, N - 1$, where BW is a signal bandwidth. We refer to the collection of these pN samples as a “snapshot”.

We assume that the bandwidth of the signal $s(t)$ is small compared to the size of the antenna array, i.e., that the propagation delays across the array are much smaller than the inverse bandwidth of the signal, so that the narrow-band array representation is applicable. This assumption is definitely valid for the bandwidth and antenna array size in modern communication techniques such as Wi-Fi.

We further assume that the antenna array is sampled M times at $\{t_m\}$, $m = 1, \dots, M$, forming M snapshots, and that the following conditions hold regarding the signals and the noise:

- A.1 The signal $s(t)$ is identical for all snapshots.
- A.2 The directions-of-arrival and the differential-delays of the multipath reflections are identical for all the M snapshots.
- A.3 The noise samples $n_i(t_m + \ell D)$; $\ell = 0, \dots, N - 1$; $m = 1, \dots, M$; $i = 1, \dots, p$ are i.i.d. Gaussian random variables with zero mean and unknown variance σ^2 .

A.1 is valid for most modern wireless communication systems, such as Wi-Fi, since these communication systems have a repeatable signal part for synchronization and channel estimation purposes. Consequently, we can confine the sampling times to this repeatable signal part using the synchronization capabilities of the receiver. A.2 is valid provided that the M snapshots are sampled in a close vicinity of each other and consequently capture the same physical environment, i.e., the same directions-of-arrival and differential-delays.

Following [26], [27], and using complex envelope representation, the ℓ -th sample of the i -th sensor can be expressed as

$$x_i(t + \ell D) = \sum_{k=1}^q \gamma_k(t) a_i(\theta_k) s(t + \ell D - \tau_k) e^{-j\omega_c \tau_k(\theta_k)} + n_i(t + \ell D) \quad (1)$$

where

- $s(t)$ is the complex envelope of the signal,
- τ_k is the delay of the k -th reflection relative to the reference,
- $\tau_i(\theta_k)$ is the delay between the i -th sensor and the reference sensor of the k -th reflection,
- $a_i(\theta_k)$ is the amplitude response of the i -th sensor to a wavefront impinging from direction θ_k ,
- $\gamma_k(t)$ is the complex coefficient representing the phase shift and attenuation of the k -th reflection,
- $n_i(t)$ is the additive noise at the i -th sensor.

It should be pointed out that our formulation assumes that (i) $\gamma_k(t)$ is fixed during a snapshot, and (ii) $\gamma_k(t)$ may vary from snapshot to snapshot. (i) is a valid assumption since the time it takes for an indoor channel to change significantly is of the order of milliseconds [28], [29], whereas the sampling duration of a snapshot $D(N-1)$ is of the order of microseconds. (ii) is a valid assumption since the time between the snapshots is of the order of milliseconds, and hence slight emitter movement or channel variations may change $\gamma_k(t)$ from snapshot to snapshot.

Using vector notation, we can rewrite (1) as follows

$$\mathbf{x}_i(t) = \mathbf{A}_i \boldsymbol{\gamma}(t) + \mathbf{n}_i(t), i = 1, \dots, p \quad (2)$$

where $\mathbf{x}_i(t)$ and $\mathbf{n}_i(t)$ are the $N \times 1$ vectors

$$\mathbf{x}_i(t) = [x_i(t), x_i(t+D), \dots, x_i(t+(N-1)D)]^T \quad (3)$$

$$\mathbf{n}_i(t) = [n_i(t), n_i(t+D), \dots, n_i(t+(N-1)D)]^T \quad (4)$$

$\boldsymbol{\gamma}(t)$ is the $q \times 1$ vector

$$\boldsymbol{\gamma}(t) = [\gamma_1(t), \dots, \gamma_q(t)]^T \quad (5)$$

and \mathbf{A}_i is the $N \times q$ matrix

$$\mathbf{A}_i = \begin{bmatrix} a_i(\theta_1) e^{-j\omega_c \tau_i(\theta_1)} \mathbf{s}(t - \tau_1), \dots, \\ a_i(\theta_q) e^{-j\omega_c \tau_i(\theta_q)} \mathbf{s}(t - \tau_q) \end{bmatrix} \quad (6)$$

with $\mathbf{s}(t - \tau_i)$ being the $N \times 1$ vector

$$\mathbf{s}(t - \tau_i) = [s(t - \tau_i), \dots, s(t + (N-1)D - \tau_i)]^T \quad (7)$$

Combining the $\mathbf{x}_i(t)$ vectors ($i = 1, \dots, p$) into the $pN \times 1$ "snapshot" vector $\mathbf{x}(t)$, we can rewrite (2) as

$$\mathbf{x}(t) = \mathbf{A} \boldsymbol{\gamma}(t) + \mathbf{n}(t) \quad (8)$$

where $\mathbf{x}(t)$ and $\mathbf{n}(t)$ are the $pN \times 1$ vectors

$$\mathbf{x}(t) = [\mathbf{x}_1^T(t), \dots, \mathbf{x}_p^T(t)]^T \quad (9)$$

$$\mathbf{n}(t) = [\mathbf{n}_1^T(t), \dots, \mathbf{n}_p^T(t)]^T \quad (10)$$

and \mathbf{A} is the $pN \times q$ matrix

$$\mathbf{A} = [\mathbf{a}(\theta_1) \otimes \mathbf{s}(t - \tau_1), \dots, \mathbf{a}(\theta_q) \otimes \mathbf{s}(t - \tau_q)] \quad (11)$$

with \otimes denoting the Kronecker product, and $\mathbf{a}(\theta_k)$ is the steering vector of the array towards direction θ_k , given by

$$\mathbf{a}(\theta_k) = [a_1(\theta_k) e^{-j\omega_c \tau_1(\theta_k)}, \dots, a_p(\theta_k) e^{-j\omega_c \tau_p(\theta_k)}]^T \quad (12)$$

We shall refer to the columns of matrix \mathbf{A} as the *direction-delay vectors* and to the span of the columns of the matrix \mathbf{A} as the *spatial-temporal signal subspace*. Note that the matrix \mathbf{A} captures all the direction-of-arrival and the differential-delay information of the multipath reflections.

As will become clear in the sequel, this spatial-temporal signal subspace will be the basis for our location fingerprint.

III. CONDITIONS FOR UNIQUE LOCALIZATION

In this section we present necessary and sufficient conditions that guarantee unique localization.

The following conditions, characterizing the array and the propagation environment, are assumed for the analysis:

- B.1 Any pN distinct direction-delay vectors are linearly independent.
- B.2 The number of reflections is smaller than the length of *direction-delay vectors*, namely $q < pN$.

We should point out that these conditions are mild and are obeyed in most practical cases.

Following (8) and ignoring the noise, since the noise is decoupled from the uniqueness problem by its nature, the M snapshots of the vector $\mathbf{x}(t)$ taken at t_1, \dots, t_M can be expressed as

$$\mathbf{X} = \mathbf{A}(\Theta, \mathbf{T}) \boldsymbol{\Gamma} \quad (13)$$

where \mathbf{X} is the $pN \times M$ matrix

$$\mathbf{X} = [\mathbf{x}(t_1), \dots, \mathbf{x}(t_M)] \quad (14)$$

$\boldsymbol{\Gamma}$ is the $q \times M$ matrix of the reflections' coefficients

$$\boldsymbol{\Gamma} = [\boldsymbol{\gamma}(t_1), \dots, \boldsymbol{\gamma}(t_M)] \quad (15)$$

and $\mathbf{A}(\Theta, \mathbf{T}) \equiv \mathbf{A}$ is the $pN \times q$ matrix defined in (11), with $\Theta = \{\theta_1, \dots, \theta_q\}$ and $\mathbf{T} = \{\tau_1, \dots, \tau_q\}$ denoting the directions-of-arrival and differential-delays of emitter reflections. Note that Θ and \mathbf{T} are the only parameters characterizing the emitter location.

Our objective is to specify necessary and sufficient conditions under which the solution $(\Theta, \mathbf{T}, \boldsymbol{\Gamma})$ of the set of (13) is unique for every batch \mathbf{X} . To this end, let η denote the rank of the $q \times M$ matrix $\boldsymbol{\Gamma}$

$$\eta = \text{rank}(\boldsymbol{\Gamma}) = \text{rank}(\boldsymbol{\Gamma} \boldsymbol{\Gamma}^H) \quad (16)$$

Following [30], [31], we can state the following:

An array satisfying conditions B.1–B.2 can uniquely localize sources having q reflections if

$$q < \frac{pN + \eta}{2} \quad (17)$$

The line of proof is analogous to [30], [31] and is based on establishing that if (17) holds true then for every \mathbf{X} we have

$$\mathbf{X} = \mathbf{A}(\Theta, \mathbf{T})\mathbf{\Gamma} \neq \mathbf{A}(\Theta', \mathbf{T}')\mathbf{\Gamma}' \quad (18)$$

for any $(\Theta', \mathbf{T}') \neq (\Theta, \mathbf{T})$ and any set of $\mathbf{\Gamma}'$. Namely, that the set of directions-of-arrival and differential-delays uniquely specifies the obtained data \mathbf{X} .

Two special cases are of the particular interest. The first case is $\eta = q$, occurring when the multipath coefficients are uncorrelated. In this case, the necessary and sufficient condition for unique localization (17) is $q < pN$. By B.2, this implies that uniqueness is always assured in this case. The second case is $\eta = 1$, occurring either when the multipath coefficients are fully correlated or in case when $M = 1$. In this case, the necessary and sufficient condition for unique localization is $q < (pN + 1)/2$.

These results show that the higher is the size pN of the spatial-temporal covariance matrix, and the higher is the rank η of the multipath coefficients matrix $\mathbf{\Gamma}$, the higher is the number q of multipath reflections the array can uniquely localize.

IV. THE ML SPATIAL-TEMPORAL SIMILARITY METRIC

To derive a similarity-metric for the fingerprint matching, we resort to the estimation of the matrix \mathbf{A} using the Maximum Likelihood (ML) criterion.

To this end, we assume that the complex attenuations $\gamma(t)$ are unknown deterministic quantities that need to be estimated in conjunction with the spatial-temporal matrix \mathbf{A} . Assuming that the received vector $\mathbf{x}(t)$ is sampled at times t_1, \dots, t_M , yielding M i.i.d. snapshots by A.3, the conditional p.d.f. of the sampled data is given by

$$p(\mathbf{x}(t_1), \dots, \mathbf{x}(t_M) | \mathbf{A}, \mathbf{\Gamma}, \sigma^2) = \prod_{m=1}^M \frac{1}{\pi^{pN} \det[\sigma^2 \mathbf{I}]} \cdot \exp\left(-\frac{1}{\sigma^2} \|\mathbf{x}(t_m) - \mathbf{A}\boldsymbol{\gamma}(t_m)\|^2\right) \quad (19)$$

The ML estimator (MLE), following [32], is given by

$$[\hat{\sigma}^2, \hat{\mathbf{A}}, \hat{\mathbf{\Gamma}}] = \arg \max_{\sigma^2, \mathbf{A}, \mathbf{\Gamma}} \left\{ -M p N \log \sigma^2 - \frac{1}{\sigma^2} \sum_{m=1}^M \|\mathbf{x}(t_m) - \mathbf{A}\boldsymbol{\gamma}(t_m)\|^2 \right\} \quad (20)$$

After straightforward derivation and elimination of constant terms, we get

$$[\hat{\mathbf{A}}, \hat{\mathbf{\Gamma}}] = \arg \min_{\mathbf{A}, \mathbf{\Gamma}} \sum_{m=1}^M \|\mathbf{x}(t_m) - \mathbf{A}\boldsymbol{\gamma}(t_m)\|^2 \quad (21)$$

Minimization now with respect to $\mathbf{\Gamma}$, yields

$$\hat{\boldsymbol{\gamma}}(t_m) = (\mathbf{A}^H \mathbf{A})^{-1} \mathbf{A}^H \mathbf{x}(t_m) \quad (22)$$

where H denotes the Hermitian conjugate.

Substituting (22) back into (21), yields

$$\begin{aligned} \hat{\mathbf{A}} &= \arg \min_{\mathbf{A}} \sum_{m=1}^M \|\mathbf{x}(t_m) - \mathbf{P}_A \mathbf{x}(t_m)\|^2 \\ &= \arg \max_{\mathbf{A}} \sum_{m=1}^M \|\mathbf{P}_A \mathbf{x}(t_m)\|^2 \end{aligned} \quad (23)$$

where \mathbf{P}_A is the projection operator onto the space spanned by the columns of the matrix \mathbf{A} .

$$\mathbf{P}_A = \mathbf{A}(\mathbf{A}^H \mathbf{A})^{-1} \mathbf{A}^H \quad (24)$$

It can be easily verified that (23) can also be written as

$$\hat{\mathbf{A}} = \arg \max_{\mathbf{A}} \text{Tr}\{\mathbf{P}_A \hat{\mathbf{R}}\} \quad (25)$$

where $\text{Tr}\{\cdot\}$ is the trace operator, and $\hat{\mathbf{R}}$ is the sample-covariance matrix

$$\hat{\mathbf{R}} = \frac{1}{M} \sum_{m=1}^M \mathbf{x}(t_m) \mathbf{x}^H(t_m) \quad (26)$$

It follows from (23) that the ML estimator of the spatial-temporal matrix \mathbf{A} is obtained by searching for the spatial-temporal signal subspace projection matrix \mathbf{P}_A that is ‘‘closest’’ to the sampled vectors $\{\mathbf{x}(t_m)\}$, $m = 1, \dots, M$, with the closeness measured by the modulus of the projection of the vectors onto this subspace.

V. SIGNAL SUBSPACE BASED LOCALIZATION

According to the ML criterion (25), the localization is carried out by searching in the database for the location i that maximizes the following expression

$$\hat{i} = \arg \max_{\{\mathbf{P}_i\}} \text{Tr}\{\mathbf{P}_i \hat{\mathbf{R}}\} \quad (27)$$

where $\hat{\mathbf{R}}$ is the sample-covariance matrix (26) and \mathbf{P}_i is the projection operator onto the signal subspace corresponding to the i -th location.

A. The Generation of the Fingerprint Database

The fingerprint database is composed of the sample-covariance and projection matrices $\{\hat{\mathbf{R}}_i, \mathbf{P}_i\}$ of all the locations and is pre-computed in the off-line phase.

The sample-covariance matrix $\hat{\mathbf{R}}_i$ is computed from L snapshots of the received vector $\mathbf{x}(t)$, collected in the close vicinity of location i . In the close vicinity of a point the directions-of-arrival and the differential-delays of the multipath reflections are essentially the same, while the coefficients vector $\boldsymbol{\gamma}(t)$ varies from location to location and may vary from snapshot to snapshot. The spatial averaging in the close vicinity of a point therefore ensures that the matrix $\mathbf{\Gamma}$ becomes full rank and hence that the full dimension of the signal subspace is captured. The spatial averaging also helps in providing a more comprehensive and robust characterization of the multipath reflections.

The expected value of $\hat{\mathbf{R}}_i$, omitting the index i for clarity of the presentation, is given by

$$\mathbf{R} = E[\mathbf{x}(t)\mathbf{x}^H(t)] = \mathbf{A}\mathbf{\Sigma}\mathbf{A}^H + \sigma^2\mathbf{I} \quad (28)$$

where

$$\mathbf{\Sigma} = E[\boldsymbol{\gamma}(t)\boldsymbol{\gamma}^H(t)] \quad (29)$$

Recalling B.2 and assuming that the $q \times q$ matrix $\mathbf{\Sigma}$ has full rank, which is a valid assumption provided that the L snapshots are collected as described above, it can be easily verified [33], [34] that the eigenvalues and eigenvectors of \mathbf{R} , denoted by $\{\lambda_1 \geq \lambda_2 \geq \dots \geq \lambda_{pN}\}$ and $\{\mathbf{v}_1, \mathbf{v}_2, \dots, \mathbf{v}_{pN}\}$, respectively, have the following important property:

The subspace spanned by the eigenvectors $\mathbf{V}_q = \{\mathbf{v}_1, \mathbf{v}_2, \dots, \mathbf{v}_q\}$ is identical to the subspace spanned by the columns of the matrix \mathbf{A} , i.e., $\text{span}(\mathbf{V}_q) = \text{span}(\mathbf{A})$.

Based on this identity, the estimation of the projection matrix $\hat{\mathbf{P}}_i$ of the i -th location is carried out as follows:

- 1) Calculate the sample-covariance matrix $\hat{\mathbf{R}}_i$ of location i by

$$\hat{\mathbf{R}}_i = \frac{1}{L} \sum_{l=1}^L \mathbf{x}(t_l)\mathbf{x}^H(t_l) \quad (30)$$

- 2) Perform an eigenvalue decomposition of $\hat{\mathbf{R}}_i$.
- 3) Estimate the signal subspace dimension \hat{q} .
- 4) Select the first \hat{q} eigenvectors of $\hat{\mathbf{R}}_i$ corresponding to the signal subspace: $\mathbf{V}_{\hat{q}} = \{\mathbf{v}_1, \mathbf{v}_2, \dots, \mathbf{v}_{\hat{q}}\}$.
- 5) Estimate the projection matrix by $\hat{\mathbf{P}}_i = \mathbf{V}_{\hat{q}}(\mathbf{V}_{\hat{q}}^H \mathbf{V}_{\hat{q}})^{-1} \mathbf{V}_{\hat{q}}^H$.

B. Signal Subspace Dimension Estimation

The estimation of the signal subspace dimension is a well-known problem in array processing and numerous techniques have been developed to solve it [33]–[35].

Yet, the problem at hand is somewhat different than the classical problem addressed in the literature. Here we are targeting a rich multipath environment, such as in indoor venues and urban canyons, where the number of reflections is usually very large, and want to ensure that the subspace dimension captures only the more dominant reflections in the environment and not the numerous low energy reflections. These low energy reflections may not be stable enough in real life scenarios because of movement of people and changing environment. To illustrate this point, refer to Fig. 2, where a typical multipath, characterizing the indoor environment shown in Fig. 3, is presented. The multipath signals originate from the location denoted by the green dot, $(x_i, y_i) = (34, 66)$ m, and captured by an antenna array at the orange dot. Fig. 2 shows the two-dimensional plot of the power of the multipath signals, parameterized by the angle-of-arrival and time-of-arrival. Note the large number of reflections and their high dynamic range, and especially the large number of low energy reflections that are close to the noise floor.

A typical profile of the eigenvalues of the covariance matrix is shown in Fig. 4. The small eigenvalues typically capture the low energy multipath reflections that should, as explained above, be

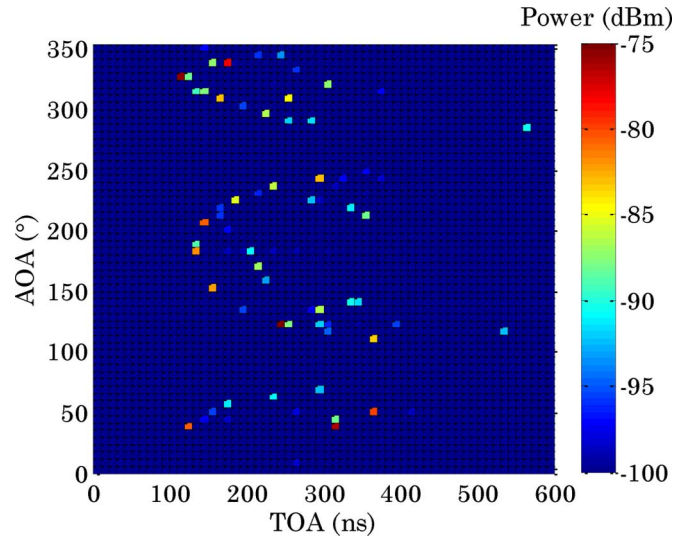


Fig. 2. The spatial-temporal power profile of the multipath reflections corresponding to the location of green dot, $(x_i, y_i) = (34, 66)$ m, in Fig. 3.

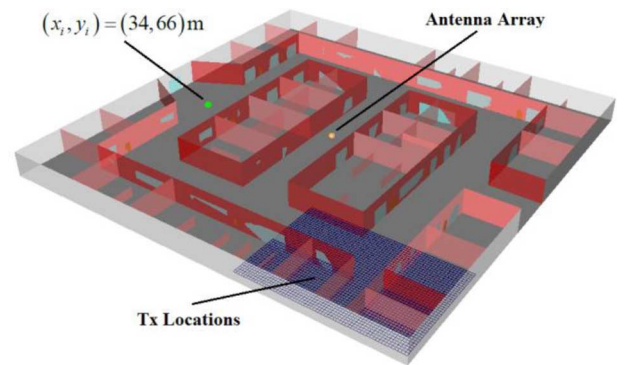


Fig. 3. The simulation environment.

excluded from the subspace formation. Based on this observation, we have disqualified the classical technique based on information theoretic criteria [36] that is sensitive to low energy signals, and selected a more robust technique that captures only the dominant reflections. Specifically, the signal subspace dimension \hat{q} is estimated by the number of large eigenvalues that capture, say, 90% of the signal energy

$$\hat{q} = \left(\min Q, \text{s.t. } \frac{\sum_{i=1}^Q \lambda_i}{\sum_{i=1}^{pN} \lambda_i} \geq \alpha \mid Q = 1, 2, \dots, pN \right) \quad (31)$$

where $\{\lambda_1 \geq \lambda_2 \geq \dots \geq \lambda_{pN}\}$ and $0 \leq \alpha \leq 1$ is a parameter set, say, to 0.9.

C. The Similarity-Profile Matching Criterion

As described above, the localization can be carried out by searching for the index i that maximizes the ML criterion (27). Yet, due to ambiguity inherent in the physical environment, some locations may have similar spatial-temporal fingerprints, and as a result give rise to a certain level of ambiguity error. To address this problem we next introduce a matching technique that better copes with these ambiguities.

To this end, following [4], we introduce the notion of similarity-profile (SP). The SP of the i -th location \mathbf{f}_i captures the

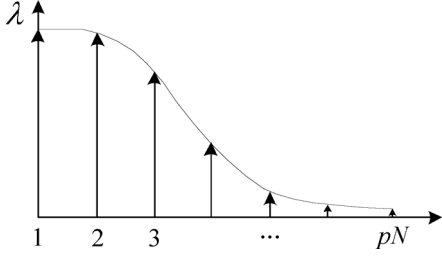


Fig. 4. A typical eigenvalue profile of the signal covariance matrix.

similarity of the received data at the i -th location to the fingerprints in the database and is defined by

$$\mathbf{f}_i = [f_{i1}, \dots, f_{iK}] \quad (32)$$

where K is the number of locations in the database and f_{ij} is the similarity between the data captured in the i -th location to the fingerprint of the j -th location

$$f_{ij} = \text{Tr}\{\mathbf{P}_j \hat{\mathbf{R}}_i\} \quad (33)$$

with

$$\hat{\mathbf{R}}_i = \hat{\mathbf{R}}_i / \text{Tr}\{\hat{\mathbf{R}}_i\} \quad (34)$$

Notice that the covariance matrices $\{\hat{\mathbf{R}}_i\}$ have been normalized to eliminate dependence on the power of the received signals. This is done to cope with potential power change of the source between the off-line and on-line phases.

The motivation for the SP matching is based on the observation that both similar and dissimilar fingerprints provide useful identification information on the query fingerprint. Consequently, it is beneficial to employ the whole similarity vector \mathbf{f}_i as the i -th location identifier.

To better illustrate this point, we refer to Fig. 5 showing the SP belonging to the green dot, $(x_i, y_i) = (34, 66)$ m, in Fig. 3. The SP vector (32) is presented as a two-dimensional plot, with color coding representing the level of similarity f_{ij} (33) between the i -th point and all the other points in the data-base. Note that this plot peaks at $(x_i, y_i) = (34, 66)$ m, as expected, but also at another point $(x, y) = (33, 10)$ m, reflecting a potential ambiguity point. To cope better with such potential ambiguities, we propose to use the whole similarity profile, with its peaks and valleys, as the fingerprint of the i -th location.

Using the SP notion we can represent the database, constructed during the off-line phase, by the similarity-matrix \mathbf{F} , given by

$$\mathbf{F} = \begin{bmatrix} \mathbf{f}_1 \\ \mathbf{f}_2 \\ \vdots \\ \mathbf{f}_K \end{bmatrix} \quad (35)$$

According to the SP criterion the localization is carried out by searching over the database \mathbf{F} for the SP that best matches the query SP obtained from the received signals. That is,

$$\hat{i} = \arg \min_{\{\text{location } i\}} \|\mathbf{f}_i - \hat{\mathbf{f}}\|_2^2 \quad (36)$$

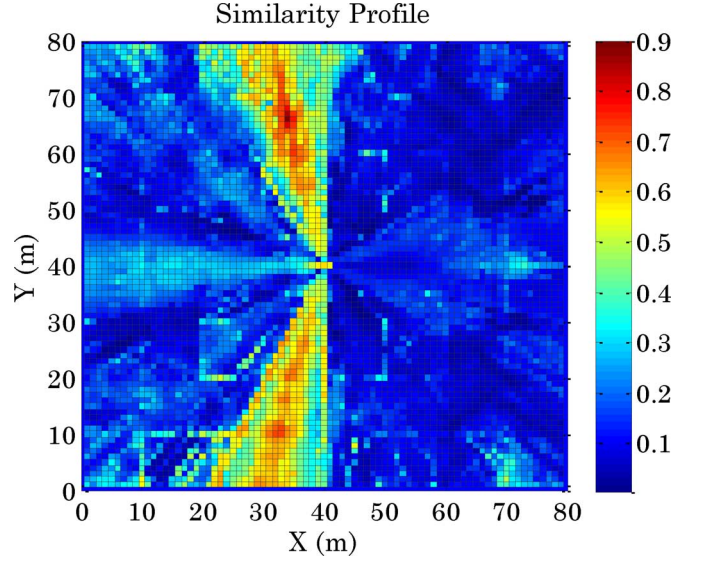


Fig. 5. The similarity profile corresponding to the location of the green dot, $(x_i, y_i) = (34, 66)$ m, in Fig. 3.

where $\hat{\mathbf{f}}$ is the query SP obtained from the received signals,

$$\hat{\mathbf{f}} = [\hat{f}_1, \dots, \hat{f}_K] = [\text{Tr}\{\mathbf{P}_1 \hat{\mathbf{R}}\}, \dots, \text{Tr}\{\mathbf{P}_K \hat{\mathbf{R}}\}] \quad (37)$$

with

$$\hat{\mathbf{R}} = \hat{\mathbf{R}} / \text{Tr}\{\hat{\mathbf{R}}\} \quad (38)$$

Note that projection matrices $\{\mathbf{P}_i\}$ and the similarity-matrix \mathbf{F} are calculated during the off-line phase, whereas $\hat{\mathbf{f}}$ is calculated in the on-line phase from the sample-covariance matrix $\hat{\mathbf{R}}$.

In the typical case, wherein $K \gg (pN)^2$, the computational load of (36) can be significantly reduced by leveraging the properties of the L_2 norm. Indeed, following [37] and using the well-known *vec* operator, which forms a column vector from the columns of a matrix by stacking them one under the other, we can write

$$\|\mathbf{f}_i - \hat{\mathbf{f}}\|_2^2 = \|\mathbf{P}(\tilde{\mathbf{r}}_i - \hat{\mathbf{r}})\|_2^2 = (\tilde{\mathbf{r}}_i - \hat{\mathbf{r}})^H \mathbf{P}^H \mathbf{P} (\tilde{\mathbf{r}}_i - \hat{\mathbf{r}}) \quad (39)$$

where

$$(\tilde{\mathbf{r}}_i - \hat{\mathbf{r}}) = (\text{vec}(\hat{\mathbf{R}}_i) - \text{vec}(\hat{\mathbf{R}})) \quad (40)$$

$$\mathbf{P} = [\text{vec}(\mathbf{P}_1^T), \dots, \text{vec}(\mathbf{P}_K^T)]^T \quad (41)$$

Assuming $\mathbf{P}^H \mathbf{P}$ has a full rank and denoting by \mathbf{G} be the Cholesky factor of $\mathbf{P}^H \mathbf{P}$, i.e.,

$$\mathbf{P}^H \mathbf{P} = \mathbf{G} \mathbf{G}^H \quad (42)$$

we can rewrite (36) as

$$\hat{i} = \arg \min_{\{\text{location } i\}} \|\mathbf{G}^H (\tilde{\mathbf{r}}_i - \hat{\mathbf{r}})\|_2^2 \quad (43)$$

Now, since \mathbf{G} is a $(pN)^2 \times (pN)^2$ matrix, as compared to \mathbf{P} which is $K \times (pN)^2$, (43) provides significant computational saving compared to (36). Indeed, in a typical scenario, with $p =$

6, $N = 4$ and $K = 10\,000$, this technique provides more than an order of magnitude savings in both the computational load and storage.

Note also that since \mathbf{G} and $\{\tilde{\mathbf{r}}_i\}$ are pre-computed in the off-line phase, the on-line computation is rather mild and involves essentially only multiplication of \mathbf{G} with $\hat{\mathbf{r}}$, the $(pN)^2$ vector of the elements of the sample-covariance matrix \mathbf{R} , and a search over the data-base for the minimum of the L_2 norm (43). We would like to point out that the computational load involved in the search over the database can be significantly reduced, by organizing the search in a tree-structured manner and leveraging the triangular inequality the L_2 norm obeys, as in [37].

VI. SIMULATION RESULTS

In this section we present simulation results illustrating the performance of the proposed localization algorithm.

To simulate a typical indoor propagation environment we used the $80\text{ m} \times 80\text{ m} \times 5\text{ m}$ shopping mall shown in Fig. 3. The mall's walls were constructed from typical materials having typical reflection and penetration coefficients. To simulate the electromagnetic propagation we used a 3D ray tracing radio wave propagation simulator. The system parameters—receiver sensitivity, transmit power and antenna gains—have been set to those typically available in off-the-shelf Wi-Fi equipment. The orange point in the center of the mall denotes the location of the antenna array. The array was a uniform circular array, with a diameter of 25 cm, having $p = 6$ omni-directional antennas. To generate the data, emitters were distributed uniformly in the mall area with 0.1 m separation. A sample of the emitter locations is shown in Fig. 3 by the blue points grid. The antenna array and the emitters were placed at a height of 2.5 m and 1.5 m, respectively.

The database was built as a rectangular grid with 1 m separation. The test points were selected by random shifts, in both axes, from the database points. That is, random shifts, Δx_i and Δy_i , were generated independently for each database point i according to a uniform distribution $U[-1/2, 1/2]m$. This was done in order to simulate a more realistic situation wherein the test points and the database points do not coincide. The sample-covariance matrices of the database and test point were constructed from L and M snapshots, respectively, captured in a close vicinity of the database/test point. The snapshots used for the database and for the test points were different.

The signal used in the simulations was the Long Training Field (LTF) of the preamble of the 802.11a/g/n Wi-Fi packet [38], which is present in each transmitted packet and is used for channel estimation, accurate frequency offset estimation and time synchronization.

The signal-to-noise ratio (SNR) varied from 0 to 60 dB according to the path loss from the base station to the emitter location and was the same in the database generation and in the tests. The eigenvalue threshold α for subspace dimension estimation (31) was selected to be 0.9 in all simulations.

The localization performance was evaluated by computing the cumulative distribution function (CDF) of the position location errors, with the position location error defined by the Euclidean distance between the location of the test point and the location of the most likely database grid point selected by the localization algorithm.

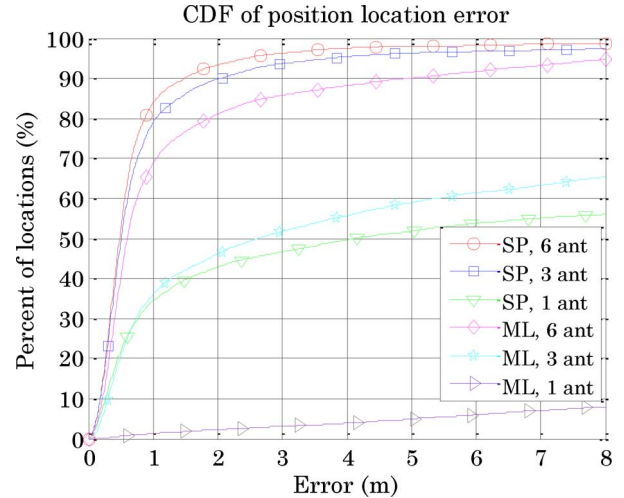


Fig. 6. Performance of the SP and ML techniques for different number of antennas. The number of taps was $N = 8$, the BW = 20 MHz and the number of snapshots for the database and tests were $L = 60$ and $M = 55$, respectively.

Simulation Scenario 1: In this simulation we present the achievable localization accuracy using the ML (27) and the SP (43) matching criteria, with a varying number of antennas. The number of samples (taps) per antenna was $N = 8$ and the signal bandwidth (BW) was 20 MHz, while the number of signal snapshots used for each database and test location were $L = 60$ and $M = 55$, respectively. To vary the number of antennas we used 3 and 1 out of the 6 antennas of the array.

As seen in Fig. 6, the accuracy difference between the SP and the ML criteria is considerable, especially in more challenging scenarios wherein the level of ambiguity increases, namely when the number of antennas is reduced from 6 to 3 and from 3 to 1. Since this advantage of the SP criterion was persistent in all the simulations, we have decided to omit the results of the ML criterion and concentrate on the SP in the sequel for clarity of the presentation.

Note also that though there is only marginal accuracy degradation when going from 6 antennas to 3, it is much more significant when going from 3 antennas to 1. This clearly demonstrates the crucial contribution of the spatial dimension in enabling high accuracy, especially at relatively low bandwidth of 20 MHz.

Simulation Scenario 2: In this simulation we present the distribution of signal subspace dimension over the mall area as a function of the number of taps N . The number of antennas was $p = 6$, the BW = 20 MHz, and the number of database snapshots $L = 60$.

As seen in Fig. 7, the signal subspace dimension rises with the increase of the dimension pN of the snapshot vector but typically stays below 9, even when the dimension of the snapshot vector rises to 24 (for $N = 4$) and 48 (for $N = 8$).

Simulation Scenario 3: In this simulation we present the influence of the number of snapshots, L and M , on the localization accuracy. The signal bandwidth was 20 MHz and the number of taps $N = 8$. In the first case (Fig. 8), the number of antennas was $p = 6$ and the number of database snapshots $L = 60$, while the number of test point snapshots varied. In the second case (Fig. 9), the number of antennas was $p = 3$ and the number

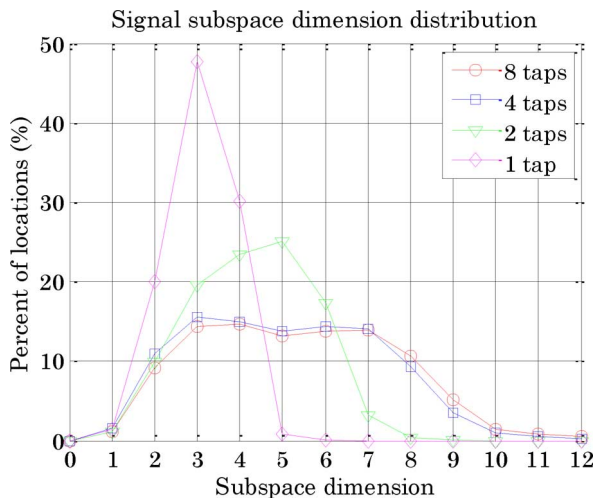


Fig. 7. Signal subspace dimension for different number of taps. The number of antennas was $p = 6$, the signal BW = 20 MHz, and the number of database snapshots $L = 60$.

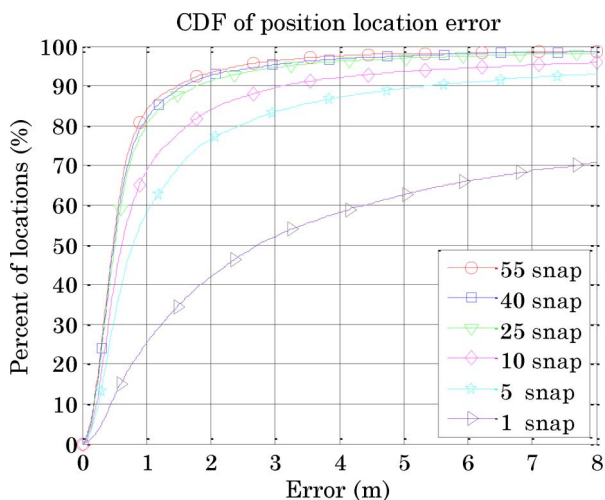


Fig. 8. Performance of the SP criterion for different number of test point snapshots. The number of antennas was $p = 6$, the BW = 20 MHz, the number of taps $N = 8$, and the number of database snapshots $L = 60$.

of test point snapshots $M = 25$, while the number of database snapshots varied.

As seen in Figs. 8 and 9, the higher the number of test point/database snapshots the higher is the accuracy. This can be attributed to the fact that the higher number of snapshots provides better covariance matrix estimation and consequently better signal subspace estimation. Yet, beyond some number of snapshots, about 25–30, the improvement in accuracy is marginal. The fact that 25–30 snapshots are sufficient to fully characterize the signal subspace can be explained by the relatively low dimension of this subspace, as discussed above and shown in Fig. 7. Since in practical applications the typical snapshot interval is of the order of milliseconds, this implies that the time necessary for localization is of the order of 100 milliseconds, which is definitely acceptable for most applications.

Simulation Scenario 4: In this simulation we present the influence of number of taps on the localization accuracy for a

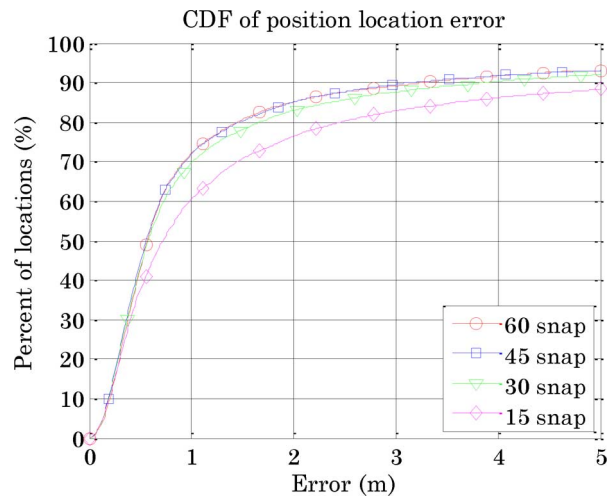


Fig. 9. Performance of the SP criterion for different number of database snapshots. The number of antennas was $p = 3$, the BW = 20 MHz, the number of taps $N = 8$, and the number of test point snapshots $M = 25$.

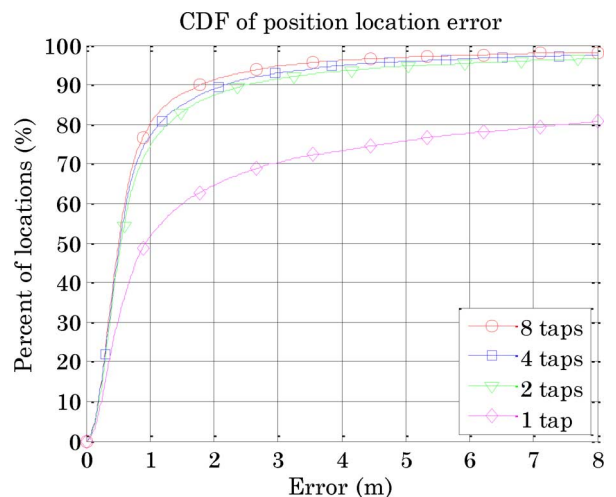


Fig. 10. Performance of the SP criterion for different number of taps. The number of antennas was $p = 6$, the BW = 20 MHz, and the number of database and test point snapshots was $L = 60$ and $M = 25$, respectively.

6-antenna array and bandwidths of 20 MHz and 80 MHz. The number of database and test point snapshots was $L = 60$ and $M = 25$, respectively.

As seen in Figs. 10 and 11, the higher is the number of taps the better is the accuracy. This can be attributed to the fact that the higher number of taps allows capturing longer-delay reflections and as a result to provide a more robust fingerprint with lower ambiguity. The improvement in accuracy for 20 MHz occurs at lower number of taps than that for 80 MHz since the sampling time for the 20 MHz and 80 MHz are 50 ns and 12.5 ns, respectively, implying that for a higher bandwidth a larger number of taps is required to capture the multipath delay spread.

Note also that in the case of a single tap there is a significant degradation in accuracy as well as much higher ambiguity level, reflected by the higher error in upper percentile of the CDF graph. This highlights the inability of spatial-only fingerprint to provide enough location distinction.

Simulation Scenario 5: In this simulation we present the achievable accuracy for a 3-antenna array using different signal bandwidths, 20 MHz, 40 MHz, and 80 MHz. The number of

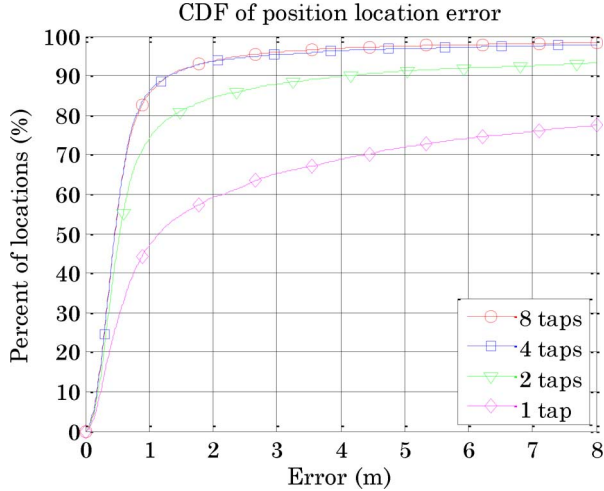


Fig. 11. Performance of the SP criterion for different number of taps. The number of antennas was $p = 6$, the BW = 80 MHz, and the number of database and test point snapshots was $L = 60$ and $M = 25$, respectively.

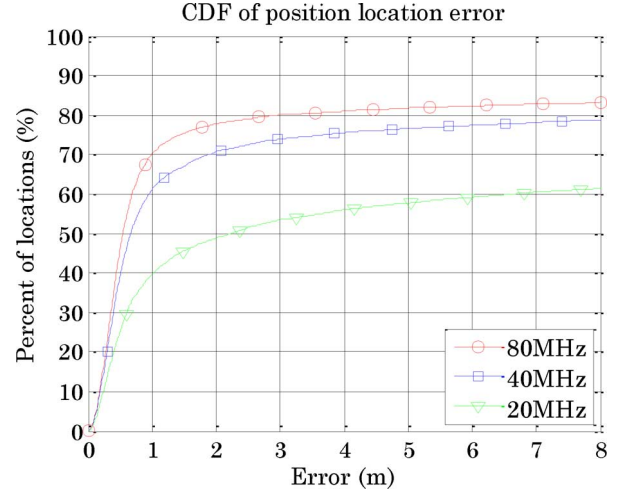


Fig. 13. Performance of the SP criterion for different BWs. The number of antennas was $p = 1$, the number of taps $N = 32$, and the number of database and test point snapshots was $L = 60$ and $M = 55$, respectively.

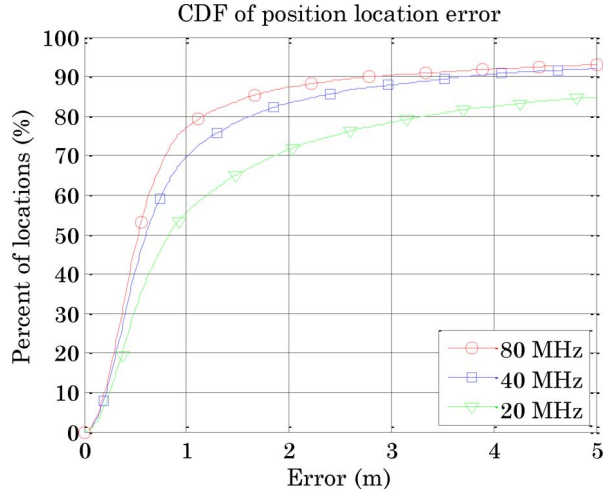


Fig. 12. Performance of the SP criterion for different BWs. The number of antennas was $p = 3$, the number of taps $N = 8$, and the number of database and test point snapshots was $L = 60$ and $M = 10$, respectively.

taps was $N = 8$, while the number of database and test point snapshots were $L = 60$ and $M = 10$, respectively.

As seen in Fig. 12, the achievable accuracy improves as the bandwidth increases. Note that the effect of the larger bandwidth is more noticeable here, as compared to that between Figs. 10 and 11, since here the scenario is more challenging—a smaller number of antennas and test point snapshots.

Simulation Scenario 6: In this simulation we present the achievable accuracy in the case of $p = 1$ antenna using different signal bandwidths, 20 MHz, 40 MHz, and 80 MHz. The simulation parameters were identical to those of scenario 1 except that here number of taps was $N = 32$.

As can be seen in Fig. 13, there is a large improvement in accuracy as the bandwidth increases, demonstrating the importance of the improved time resolution resulting from the increased bandwidth in the case of single antenna.

Note also that the ambiguity level, reflected by the higher error in upper percentile of the CDF graph, is considerably

higher than in the case of 6 and 3 antennas presented in Fig. 6. This high level of ambiguity highlights the inability of temporal-only fingerprint to provide enough location distinction.

VII. REAL DATA RESULTS

In this section we present experimental results illustrating the performance of the proposed localization algorithm with real data.

The experiment was conducted at the 33 m \times 33 m \times 5 m of-office floor shown in Fig. 14. The BS was an 802.11g Wi-Fi access point (AP) having a uniform circular array, with a diameter of 25 cm and $p = 6$ omni-directional antennas. The antenna array was located at the red dot. The emitter was a laptop communicating with the BS over Wi-Fi. The antenna array and the emitter were placed at a height of 3 m and 1.5 m, respectively. The green square points, separated by 0.5 m, denote locations of database points. The database covariance matrices were built by spatial averaging of the captured data in the vicinity of these points. The test point locations were selected by random shifts from the database points, in a similar way to the simulations.

To enable performance comparison with simulated data in both the experiment and simulation we used $p = 6$ antennas, BW of 20 MHz, $N = 8$ taps, and $L = 30$ for the database and $M = 25$ for the test points. The eigenvalue threshold α for subspace dimension estimation (31) was selected to be 0.9. The signal used was the long training field (LTF) of the preamble of the 802.11g Wi-Fi packet [38] with BW = 20 MHz.

As seen in Fig. 15, the accuracy achieved with real data is about 1 m and closely matches that obtained with the simulated data. This clearly validates the proposed method and the simulation results.

VIII. DISCUSSION

In this section we discuss several aspects affecting the localization accuracy.

It should be clear from the simulations that given a rich multipath environment, the localization accuracy is a function of

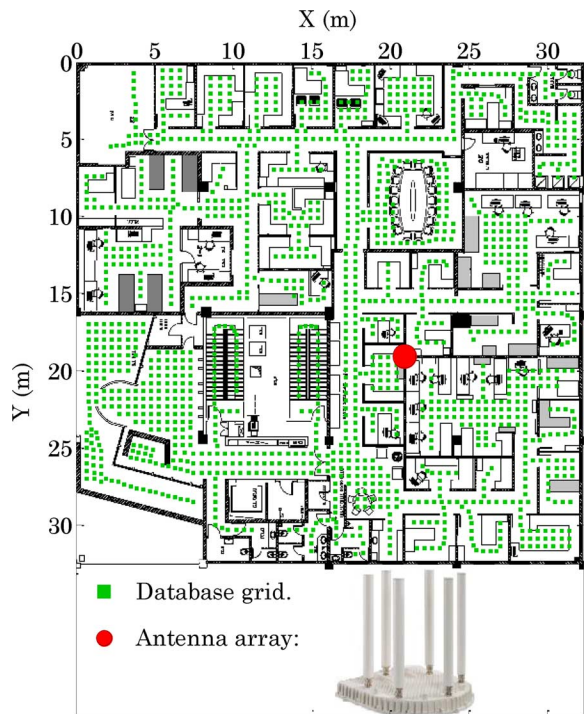


Fig. 14. The office floor wherein the real data experiment was conducted.

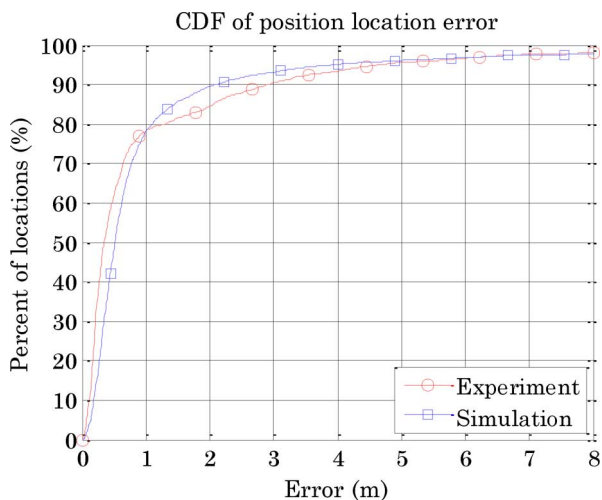


Fig. 15. Performance of the SP criterion for real data compared to that of simulated data. In both we used $p = 6$ antennas, 20 MHz BW, $N = 8$ taps, and the number of database and test point snapshots was $L = 30$ and $M = 25$ respectively.

many system parameters including the antenna array size, the number of antenna elements, the BW of the signal, the number of taps, the number of snapshots used for the database grid and the number of snapshots used for the test points. As seen in the simulations, these system parameters can be traded, up to a degree, to compensate for each other.

The localization accuracy can be improved by either using some sort of interpolation between the database grid points or by using a finer grid. Yet, the improvement in accuracy has its limit, dictated by the system parameters and by the noise level characterizing the environment and the database generation.

The accuracy is affected also by the value of the parameter α used for the subspace dimension estimation. The higher is α the higher is the estimated dimension and hence the richness of the fingerprint. We have found that varying α in the range 0.8–0.9 has mild effect on the accuracy and that 0.9 presents overall the best performance, serving as a good compromise between the conflicting desires for enriching the fingerprint, on the one hand, and for robustness of the fingerprint, on the other hand.

Last, but not least, it should be clear that in case an area is covered by more than one base station, using all the information from the overlapping base stations should improve the localization accuracy. Naturally, there are several ways to exploit the overlapping coverage, with varying level of computational load and accuracy.

IX. CONCLUSION

We have presented a novel method enabling single-site localization based on a spatial-temporal fingerprint of the multipath reflections. This spatial-temporal fingerprint is based on a lower dimensional subspace of the spatial-temporal covariance matrix—referred to as the signal subspace—capturing the directions-of-arrival and the differential-delays of the dominant multipath reflections. The fingerprint matching is based on the SP criterion, which outperforms considerably the conventional ML criterion, especially in challenging scenarios that are prone to ambiguity.

The high level of accuracy of this method, demonstrated by simulations and real data results, and its mild computational load, make it a promising candidate for providing high quality and ubiquitous localization in indoor environments.

APPENDIX

In this Appendix we show that our method is applicable also to localization using the array channel impulse response (CIR).

In modern communication systems the CIR is usually obtained by exploiting a known signal, referred to as training signal, specifically included in the transmitted signal for this purpose. The CIR is obtained by de-convolution of the received signal with this training signal.

It follows from the problem formulation presented in Section II above that the ℓ -th sample of the estimated CIR corresponding to the i -th sensor and m -th snapshot can be expressed by

$$\hat{h}_i(t_m + \ell D) = \sum_{k=1}^q \gamma_k(t_m) a_i(\theta_k) \times g(t_m + \ell D - \tau_k) e^{-j\omega_c \tau_i(\theta_k)} + n_i(t_m + \ell D) \quad (44)$$

where $g(t)$ is the convolution of the transmit and receive filters and $n_i(t + \ell D)$, $\ell = 0, \dots, N - 1$ are samples of the CIR estimation noise. We assume that the estimation noise conforms to the assumption A.3.

Note that expression (1) and (44) are essentially identical, differing only in the signal part. Yet, since $g(t)$ is repeatable from snapshot to snapshot, A.1–A.2 apply here as well.

Stacking the estimated CIR samples in a vector form analogously to (9), we get

$$\hat{\mathbf{h}}(t) = \mathbf{A}\boldsymbol{\gamma}(t) + \mathbf{n}(t) \quad (45)$$

Since this expression is identical to our problem formulation (8), we can straightforwardly apply our localization method to the sample-covariance of the array CIR, given by

$$\hat{\mathbf{C}} = \frac{1}{M} \sum_{m=1}^M \hat{\mathbf{h}}(t_m) \hat{\mathbf{h}}^H(t_m) \quad (46)$$

Note that our localization method differs from the PDP methods in two aspects. First, its fingerprint is based on the signal subspace spanned by the dominant reflections. Second, its matching algorithm is based on the SP criterion.

The advantage of using the CIR for localization, as compared to using the received signals with a repeatable part, is the indifference of the localization algorithm to different repeatable parts (training signals). Yet, its computational load, in both the off-line and on-line phases, is higher because of the extra de-convolution step required to obtain the CIR estimates.

ACKNOWLEDGMENT

The authors are grateful to the reviewers for their valuable comments and suggestions.

REFERENCES

- [1] A. H. Sayed, A. Tarighat, and N. Khajehnouri, "Network-based wireless location," *IEEE Signal Process. Mag.*, vol. 22, no. 4, pp. 24–40, Jul. 2005.
- [2] G. Sun, J. Chen, W. Guo, and K. J. R. Liu, "Signal processing techniques in network-aided positioning," *IEEE Signal Process. Mag.*, vol. 22, pp. 12–23, Jul. 2005.
- [3] O. Hilsenrath and M. Wax, "Radio transmitter location finding for wireless communication network service and management," U.S. Patent 6 026 304, Feb. 2000.
- [4] M. Wax, Y. Meng, and O. Hilsenrath, "Subspace signature matching for location ambiguity resolution in wireless communication systems," U.S. Patent 6 064 339, May 2000.
- [5] M. Wax and O. Hilsenrath, "Signature matching for location determination in wireless communication systems," U.S. Patent 6 112 095, Aug. 2000.
- [6] M. Wax, O. Hilsenrath, and A. Bar, "radio transmitter location finding in CDMA wireless communication systems," U.S. Patent 6 249 680, Jun. 2001.
- [7] M. Nezafat, M. Kaveh, H. Tsuji, and T. Fukagawa, "Localization of wireless terminals using subspace matching with ray-tracing-based simulations," in *Proc. IEEE SAM*, Jul. 2004, pp. 623–627.
- [8] M. Nezafat, M. Kaveh, H. Tsuji, and T. Fukagawa, "Subspace matching localization: A practical approach to mobile user localization in micro-cellular environments," in *Proc. IEEE Veh. Technol. Conf. (VTC)*, Sep. 2004, vol. 7, pp. 5145–5149.
- [9] M. Nezafat, M. Kaveh, and H. Tsuji, "Indoor localization using a spatial channel signature database," in *Proc. IEEE AWPL*, Dec. 2006, vol. 5, pp. 406–409.
- [10] H. Koshima and J. Hoshen, "Personal locator services emerge," *IEEE Spectrum Mag.*, vol. 37, no. 2, pp. 41–48, Feb. 2000.
- [11] P. Bahl and V. N. Padmanabhan, "RADAR: An in-building RF-based user location and tracking system," in *Proc. IEEE INFOCOM*, Mar. 2000, vol. 2, pp. 775–784.
- [12] H. Laitinen, J. Lahteenmaki, and T. Nordstrom, "Database correlation method for GSM location," in *Proc. IEEE Veh. Technol. Conf. (VTC)*, 2001, vol. 4, pp. 2504–2508.
- [13] T. Nypan, K. Gade, and O. Hallingstad, "Vehicle positioning by database comparison using the box-cox metric and Kalman filtering," in *Proc. IEEE Veh. Technol. Conf. (VTC)*, May 2002, vol. 4, pp. 1650–1654.
- [14] S. Ahonen and H. Laitinen, "Database correlation method for UMTS location," in *Proc. IEEE Veh. Technol. Conf. (VTC)*, Apr. 2003, vol. 4, pp. 2696–2700.
- [15] S. Ahonen and P. Eskelinen, "Mobile terminal location for UMTS," *IEEE Aerosp. Electron. Syst. Mag.*, vol. 18, no. 2, pp. 23–27, Feb. 2003.
- [16] M. Meurer, S. Heilmann, D. Reddy, T. Weber, and P. W. Baier, "A signature based localization technique relying on covariance matrices of channel impulse responses," in *Proc. WPNC & UET*, 2005, pp. 31–40.
- [17] M. Triki and D. T. M. Slock, "Mobile terminal positioning via power delay profile fingerprinting: Reproducible validation simulations," in *Proc. IEEE Veh. Technol. Conf. (VTC)*, Sep. 2006, pp. 1–5.
- [18] M. Triki and D. T. M. Slock, "Mobile localization for NLOS propagation," in *Proc. IEEE PIMRC*, Sep. 2007, pp. 1–4.
- [19] T. Oktem and D. T. M. Slock, "Power delay Doppler profile fingerprinting for mobile localization in NLOS," in *Proc. IEEE PIMRC*, Sep. 2010, pp. 876–881.
- [20] T. Oktem and D. Slock, "Cramer-Rao bounds for power delay profile fingerprinting based positioning," in *Proc. IEEE Int. Conf. Acoust., Speech, Signal Process. (ICASSP)*, May 2011, pp. 2484–2487.
- [21] T. Oktem and D. Slock, "Pairwise error probability analysis for power delay profile fingerprinting based localization," in *Proc. IEEE Veh. Technol. Conf. (VTC)*, May 2011, pp. 1–5.
- [22] F. Althaus, F. Troesch, and A. Wittneben, "UWB geo-regioning in rich multipath environment," in *Proc. IEEE Veh. Technol. Conf. (VTC)*, Sep. 2005, vol. 2, pp. 1001–1005.
- [23] C. Steiner and A. Wittneben, "Low complexity location fingerprinting with generalized UWB energy detection receivers," *IEEE Trans. Signal Process.*, vol. 58, no. 3, pp. 1756–1767, Mar. 2010.
- [24] C. Steiner and A. Wittneben, "Efficient training phase for ultrawideband-based location fingerprinting systems," *IEEE Trans. Signal Process.*, vol. 59, no. 12, pp. 6021–6032, Dec. 2011.
- [25] R. Talmon, I. Cohen, and S. Gannot, "Supervised source localization using diffusion kernels," in *Proc. IEEE WASPAA*, Oct. 2011, pp. 245–248.
- [26] M. Wax, T. J. Shan, and T. Kailath, "Spatio-temporal spectral analysis by eigenstructure methods," *IEEE Trans. Acoust., Speech, Signal Process.*, vol. 32, no. 4, pp. 817–827, Aug. 1984.
- [27] M. Wax and A. Leshem, "Joint estimation of time delays and directions of arrival of multiple reflections of a known signal," *IEEE Trans. Signal Process.*, vol. 45, no. 10, pp. 2477–2484, Oct. 1997.
- [28] D. Tse and P. Viswanath, *Fundamentals of Wireless Communication*. New York: Cambridge Univ. Press, 2005, pp. 10–42.
- [29] E. Perahia, A. Sheth, T. Kenney, R. Stacey, and D. Halperin, "Investigation into the Doppler component of the IEEE 802.11n channel model," in *Proc. IEEE GLOBECOM*, Dec. 2010, pp. 1–5.
- [30] I. Ziskind and M. Wax, "On unique localization of multiple sources by passive sensor arrays," *IEEE Trans. Acoust., Speech, Signal Process.*, vol. 37, no. 7, pp. 996–1000, Jul. 1989.
- [31] A. L. Swindlehurst, "Time delay and spatial signature estimation using known asynchronous signals," *IEEE Trans. Signal Process.*, vol. 46, no. 2, pp. 449–462, Feb. 1998.
- [32] M. Wax and I. Ziskind, "Maximum likelihood localization of multiple sources by alternating projection," *IEEE Trans. Acoust., Speech, Signal Process.*, vol. 36, no. 10, pp. 1553–1560, Oct. 1988.
- [33] R. O. Schmidt, "Multiple emitter location and signal parameter estimation," *IEEE Trans. Antennas Propag.*, vol. 34, no. 3, pp. 276–280, Mar. 1986.
- [34] H. Krim and M. Viberg, "Two decades of array processing research: The parametric approach," *IEEE Signal Process. Mag.*, vol. 13, no. 4, pp. 67–94, Jul. 1996.
- [35] H. L. Van Trees, *Optimum Array Processing: Detection, Estimation, and Modulation Theory*. New York: Wiley, 2002.
- [36] M. Wax and T. Kailath, "Detection of signals by information theoretic criteria," *IEEE Trans. Acoust., Speech, Signal Process.*, vol. ASSP-33, no. 2, pp. 387–392, Apr. 1985.
- [37] M. Wax, S. Jayaraman, V. Radionov, G. Lebedev, and O. Hilsenrath, "Efficient storage and fast matching of wireless spatial signatures," U.S. Patent 6 104 344, Aug. 2000.

- [38] E. Perahia and R. Stacey, *Next Generation Wireless LANs*. New York: Cambridge Univ. Press, 2008, p. 61, 107.



Evgeny Kupershtein received the B.Sc. degree in electrical engineering from the Technion, Israel Institute of Technology, Haifa, Israel, in 2007. He is currently pursuing the M.Sc. degree in electrical engineering at the Technion.

From 2006 to 2009, he worked as an engineer in the Israel Defense Forces. Since 2010, he has been with Wavion Wireless Networks, Israel. His research interests include signal processing, wireless communication and position location.



Mati Wax (S'84–M'84–SM'88–F'94) received the B.Sc. and M.Sc. degrees from the Technion, Israel Institute of Technology, Haifa, Israel, in 1969 and 1975, respectively, and the Ph.D. degree from Stanford University, Stanford CA, in 1985, all in electrical engineering.

From 1969 to 1973, he served as an electronic engineer in the Israeli Defense Forces. During 1974 he was with A.E.L., Israel. From 1975 to 1980 he was in Rafael, Israel, where he led the development of wireless surveillance systems. In 1984 he was a visiting scientist in IBM Almaden Research Center, San Jose, CA. From 1985 to 1996, he worked in Rafael, Israel, where he founded and headed the Center for Signal Processing, focusing on the application of multiple-antenna signal processing to wireless communication and position location. From 1997 to 1999, he was Co-Founder and CTO of US Wireless, San Ramon, CA, where he led the development of a multiple-antenna location fingerprinting technology for position location. From 2000 to 2011, he was the Founder and CTO of Wavion, Israel, where he was responsible for the development of multiple-antenna communication systems for wireless broadband access. Since 2012, following the acqui-

sition of Wavion by Alvarion, Israel, he is the CTO of Alvarion. His research interests include signal processing and wireless communications.

Dr. Mati is a recipient of the Israel Defense Award from the President of Israel, in 1981, and the Senior Paper Award of the IEEE TRANSACTIONS ON ACOUSTICS, SPEECH AND SIGNAL PROCESSING in 1985.



Israel Cohen (M'01–SM'03) is an Associate Professor of electrical engineering at the Technion—Israel Institute of Technology, Haifa, Israel. He received the B.Sc. (*summa cum laude*), M.Sc. and Ph.D. degrees in electrical engineering from the Technion—Israel Institute of Technology, in 1990, 1993 and 1998, respectively.

From 1990 to 1998, he was a Research Scientist with RAFAEL Research Laboratories, Haifa, Israel Ministry of Defense. From 1998 to 2001, he was a Postdoctoral Research Associate with the Computer Science Department, Yale University, New Haven, CT. In 2001 he joined the Electrical Engineering Department of the Technion. His research interests are statistical signal processing, analysis and modeling of acoustic signals, speech enhancement, noise estimation, microphone arrays, source localization, blind source separation, system identification and adaptive filtering. He is a coeditor of the Multichannel Speech Processing section of the *Springer Handbook of Speech Processing* (Springer, 2008), a coauthor of *Noise Reduction in Speech Processing* (Springer, 2009), a coeditor of *Speech Processing in Modern Communication: Challenges and Perspectives* (Springer, 2010).

Dr. Cohen is a General Co-Chair of the 2010 International Workshop on Acoustic Echo and Noise Control (IWAENC). He is a recipient of the Alexander Goldberg Prize for Excellence in Research, and the Muriel and David Jacknow award for Excellence in Teaching. He served as Associate Editor of the IEEE TRANSACTIONS ON AUDIO, SPEECH, AND LANGUAGE PROCESSING and IEEE SIGNAL PROCESSING LETTERS, and as Guest Editor of a *EURASIP Journal on Advances in Signal Processing* Special Issue on Advances in Multimicrophone Speech Processing and an *Elsevier Speech Communication Journal* Special Issue on Speech Enhancement.